J Solid State Electrochem (2002) 6: 237–244
DOI 10.1007/s100080100225

ORIGINAL PAPER

H. Cesiulis · A. Baltutiene · M. Donten · M.L. Donten
Z. Stojek

Increase in rate of electrodeposition and in Ni(II) concentration in the bath as a way to control grain size of amorphous/nanocrystalline Ni-W alloys

Received: 26 March 2001 / Accepted: 15 May 2001 / Published online: 21 July 2001

Abstract Calculations based on the equilibria involved have been carried out to find the conditions of the highest possible solubility of Ni(II) in an ammonia-citrate bath for the electrodeposition of amorphous/nanocrystalline Ni-W alloys. The appropriate increase in the concentration of citrate, followed by the corresponding increase in the concentration of Ni(II), has led, under the conditions of constant current, to the increase in the efficiency of the electrodeposition and therefore the rate of electrodeposition by 3.2 times. The amorphous alloys obtained in solutions of different Ni(II) concentrations had different sizes of nanocrystals (15–100 Å), as determined from X-ray diffractograms, and different alloy compositions (10–19.5 at% of W), but were of similar high hardness.

Keywords Amorphous alloys · Nanocrystals · Nickel-tungsten alloy · Electrodeposition · Ammonium citrate bath

Introduction

Tungsten alloys with iron [1, 2], cobalt [1, 3, 4, 5, 6] and nickel [1, 2, 7, 8, 9, 10] can be obtained in the amorphous state by electrodeposition. In fact, this is not an ideal amorphousness. The corresponding X-ray diffractograms do exist; however, they usually have just one very wide diffraction peak. The thickness of the peak measured at one half of its maximum intensity, $\Delta 2\theta$, often exceeds 6°. Recently, the word "amorphous" is often replaced by the word "nanocrystalline", as it is believed that nanocrystals are responsible for the X-ray peaks of amorphous materials [11].

The amorphous alloys of W with the iron group metals exhibit some remarkable exploration properties such as high corrosion resistance [2], premium hardness [1, 2, 3] and high resistance to wear [2, 4, 7]. These attractive properties made the mechanical, motor and electronic industries focus their interest on W amorphous alloys, especially the one with Ni. This alloy has a noble appearance and is seen as a potentially environmentally safe substitute for hard chromium plating and a new material for the microelectronics and microelectromechanical systems (MEMS) technologies [7].

For the electrodeposition of the tungsten alloys we have been using citric-ammonia solution, which is a modification of the inefficient primary bath containing a difficult to handle salt, boron phosphate [4, 5, 6, 12]. In this medium, a very good quality of the coatings can be obtained, and by using the appropriate current pulsing the content of tungsten (in the Co-W alloy) can be raised up to 41 at%. An increase in the tungsten content can be also obtained by eliminating ammonia from the bath [8]. Interestingly, a substantial increase in the ductility of the Ni-W alloy can be obtained by removing, under vacuum, the hydrogen dissolved in the alloy [13]. Our recent finding was that a mixed Ni-Fe-W amorphous alloy deposited from the citric-ammonia bath appeared to give the best properties for the Ni-W and Fe-W alloys [14].

Both the current efficiency and the rate of the electrodeposition of the Ni-W amorphous alloys from the citric bath are disappointingly low. The current efficiency usually does not exceed 12–14%. Two reasons for such a low efficiency can be given: (1) hydrogen evolution during the electrodeposition process; (2) the low solubility of $NiSO_4$ in the bath. The second point has particularly attracted our attention. The aim of this work was to modify the citric-ammonia bath composition so that the Ni(II) concentration and the rate of growth of

M.L. Donten is on a science project from Juliusz Slowacki VII High School, ul. Wawelska 46, Warsaw, Poland

M. Donten · M.L. Donten · Z. Stojek (✉)
Department of Chemistry, University of Warsaw,
ul. Pasteura 1, 02-093 Warsaw, Poland
E-mail: stojek@chem.uw.edu.pl

H. Cesiulis · A. Baltutiene
Department of Physical Chemistry, Vilnius University,
Naugarduko 24, 2006 Vilnius, Lithuania

the Ni-W alloy films could be increased. This was accomplished by using thermodynamic optimization. The alloys obtained were examined to find out how the increase in the deposition rate would affect the amorphousness and the composition of the Ni-W alloy.

Experimental

Current density was controlled using a Russian programmable PI-50-1.1 galvanostat/potentiostat. The deposition time varied from 30 to 120 min. For the electrodeposition a plating cell with two separated anodic compartments was used. The anodes were two plain graphite rods of area ca. 10 cm^2 each. The substrates were made of pure copper foil of working area 2 cm^2. Immediately before plating they were degreased and then slightly etched/activated with dilute sulfuric acid. An optimal current density of 70 mA/cm^2 and an optimal bath temperature of 65 °C, as reported in previously [6], were used.

The bath composition improved and optimized for the electrodeposition of Ni-W alloys [6] was the starting point in this work and is called the initial solution throughout this paper. This solution contains 0.265 mol/dm^3 Na_2WO_4, 0.135 mol/dm^3 sodium citrate (Na_2H_2Cit), 0.065 mol/dm^3 citric acid (H_4Cit), 0.014 mol/dm^3 H_3PO_4, 0.4 mol/dm^3 H_3BO_4 and 0.02 mol/dm^3 $NiSO_4$. Ammonia water was used to keep the pH at its optimal value of 8.5, and 2-butene-1,4-diol (50 mg/dm^3) and rokafenol N-10 (nonionic detergent similar to Lutensol) (100 $\mu l/dm^3$) were added as brightener and wetting agent, respectively. The changes introduced in the course of the work concerned the concentration of Ni(II) and/or the sum of the $Na_2H_2Cit + H_4Cit$ concentrations only.

Spectrophotometric investigations were carried out with a spectrophotometer, type KFK-2MP (LOMO, Russia). The solutions for these investigations were prepared by adding various amounts of the working $NiSO_4$ solution to a series of 25 mL standard flasks. NaOH and water were added to adjust pH and volume, respectively. All the solutions were equilibrated in a thermostat.

The composition of the deposits was examined using a Roentec (model M1) EDX analyzer (Germany) assembled with a LEO 435 VP scanning electron microscope. The structure of the deposits was determined by the X-ray diffraction method using a DRON-1 instrument equipped with a Fe X-ray tube (K_α: $\lambda = 1.9373$ Å). The alloy layers were not separated from the copper substrate before the X-ray measurements.

The buffer capacity of the plating bath solution was determined by titration with a 9.73 mol/dm^3 NaOH solution to avoid any dilution effects. Changes in pH were monitored with a pH meter, type MP220 (Switzerland). CurveExpert software (produced by Daniel Hyams) was used for the extraction of buffer capacity from the titration curves, and Maple V software (Waterloo Maple Software and University of Waterloo) was adopted for the calculations of the distribution of the species.

All solutions were prepared using reagent grade chemicals and doubly distillated water.

Results and discussion

Experimental and theoretical study of the solubility of Ni(II) in the plating bath solution

Since the solutions containing Ni(II) are colored, it was possible to estimate the Ni(II) concentration and its solubility in the bath by spectrophotometric measurements. For this study we have used the initial solution with varying amounts of $NiSO_4$ added to it. The experimental spectrophotometric data obtained, plotted as absorbance versus Ni(II) concentration, are shown in Fig. 1. Absorbance of the freshly prepared solutions versus concentration of Ni(II) is approximately linear over the entire concentration range. A small amount of greenish precipitate was obtained only in the solutions containing Ni(II) at a concentration of 0.09 mol/dm^3. After longer times (usually after 24 h) and for concentrations of Ni(II) higher than 0.030 mol/dm^3, the appearance of a precipitate in the solution was always observed. This phenomenon was accompanied by a decrease in the absorbance in the visible light, so it was clear that the effect is caused by the decrease of the Ni(II) amount in the solutions.

During the experiments the solutions were not decanted; therefore they were in equilibrium with the solid phase. The shape of the spectra did not qualitatively change as the solution aged, which means that the precipitation was the only change in the solution. The precipitation of two insoluble nickel compounds, phosphate and hydroxide, was considered. It was found by X-ray fluorescence analysis of the precipitate that nickel precipitated from the solution as $Ni_3(PO_4)_2$. The solubility of Ni(II), *S*, in the bath (initial solution), estimated from the experimental data, is 0.025–0.03 mol/dm^3. The final value for the Ni(II) solubility was usually established in approximately 10 days.

To identify the factors that influence Ni(II) solubility, mathematical simulations of the distribution of all the species in the bath were performed. For this purpose a complete set of equations related to all equilibria in the solution was solved. This set included the following re-

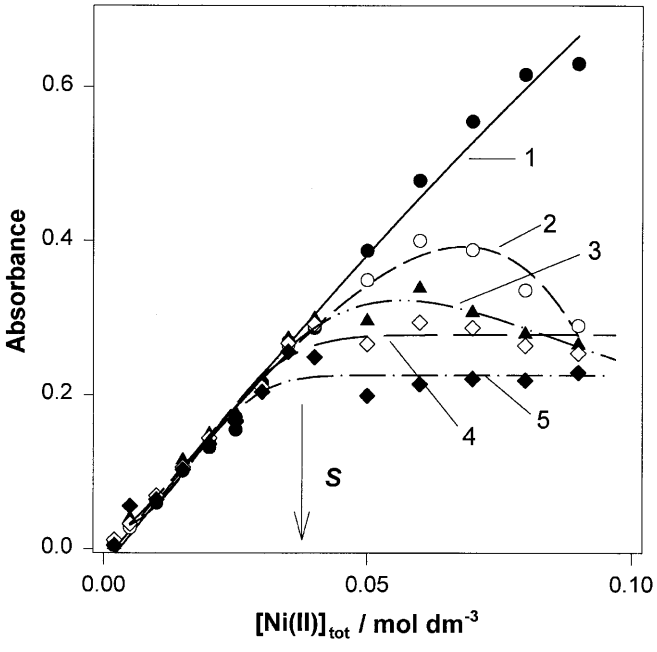

Fig. 1 Absorbance plotted versus total concentration of Ni(II) in the initial solution. Measurement time: immediately after preparation (*1*); after 24 h (*2*); after 48 h (*3*); after 68 h (*4*); after 240 h (*5*). Wavelength: 670 nm

lations and quantities: the equilibrium constants for all compounds added to or formed in the solution (e.g. the dissociation constants for the acids and ammonia and the stability constants for various nickel complexes); the mass balance, $[J]_{total} = \sum \left[J_i^{n+/-}\right]$, for all forms in the equilibrium mixture; and the charge balance, $\sum n_i \left[\mathrm{Cat}_i^{n+}\right] = \sum n_i \left[\mathrm{An}_i^{n-}\right]$, where "Cat" and "An" denote cation and anion, respectively.

Because the precipitate formed during the aging process was identified as nickel phosphate, the solubility product of $Ni_3(PO_4)_2$ was taken as the condition for the saturation of the solution by Ni(II). The formation of the following mononuclear nickel complexes was taken into account in the calculations: $NiOH^+$, $Ni(OH)_2$, $Ni(OH)_3^-$, $NiHCit^-$, $NiCit^{2-}$, $Ni(HCit)_2^{4-}$, $NiHPO_4$ and $Ni(NH_3)_n^{2+}$, where $n = 1$–6. It is worth noting that an appreciable amount of $NiCit^{2-}$ is obtained at pH values higher than 10–11 for an ionic strength of 2 mol/dm^3, whereas in solutions of low ionic strength a pH value of 13–15 is needed to obtain a significant quantity of the complex. The formation of multinuclear complexes, which were reported to exist in extremely small quantities in the concentrated citrate solutions [15], was neglected. The nickel mixed complexes (with two different ligands) cannot be formed in significant quantities [16] and were not considered in the calculations either.

The system Ni(II)-citrates-ammonia-phosphates

The calculation of the distribution of the nickel complexes in a solution containing various ligands is not straightforward, since most of the values of the stability constants are reported for low ionic strength and for low concentrations of metal and ligand. At the same time, the majority of plating solutions have high concentrations of the ionic species.

As reported above, the maximum concentration of Ni(II) in the plating bath solution was ca. 0.025 mol/dm^3. The distribution of the Ni(II) species in the plating bath solution saturated with Ni(II) was calculated using five sets of stability constants from different sources [17, 18, 19, 20]. In all cases the dominating species appeared to be the same, and its calculated concentrations were similar. However, the differences in the concentrations of the minor components were significant, e.g. they differed by more than three orders of magnitude in the case of $Ni(OH)^+$. If the results of the calculations for the saturated solutions were correct, the calculated value of the concentration product $\left[Ni^{2+}\right]^3\left[PO_4^{3-}\right]^2$ would be close to the solubility product of $Ni_3(PO_4)_2$, i.e. $K_{s0} = 10^{-30.3}$ [20]. Not surprisingly, the data, which were obtained without making corrections for the high ionic strength, gave values for the concentration product departing by five orders of magnitude from the solubility product.

The ionic strength of the bath was estimated by us to be equal to 2 mol/dm^3, and for this number the activity coefficients of all ions were calculated. The results for the distribution of the ions done for two selected sets of the stability constants and corrected for the changes in the activity coefficients are presented in Table 1. It can be seen that the concentration product $\left[Ni^{2+}\right]^3\left[PO_4^{3-}\right]^2$ is much closer to the solubility product in the case of corrected stability constants.

The distribution of all the species containing Ni(II) as a function of pH is shown in Fig. 2. In the pH range from 8 to 10, which is recommended for the plating process, the dominating species in the bath are the citrate and ammonia complexes. The molar fractions of

Table 1 Concentrations of Ni(II) complexes in the solution saturated with $NiSO_4$ calculated with the use of various sets of stability constants. Solution composition: total Ni(II) concentration = 0.025 mol/dm^3, $C_{\mathrm{Cit,tot}} = 0.2$ mol/dm^3, $[H_3PO_4] = 0.014$ mol/dm^3, $[H_3BO_3] = 0.365$ mol/dm^3; $[NH_3]_{\mathrm{tot}} = 0.415$ mol/dm^3

Particle	Concentration of species (mol/dm^3)		
	Stability constants taken from [19]; ionic strength 0.25 mol/dm^3	Stability constants taken from [20]; ionic strength 0–0.1 mol/dm^3	Stability constants taken from [20]; corrected for ionic strength 2 mol/dm^3
$Ni(HCit)_2^{4-}$	0.02463	0.0236	0.0244
$NiCit^{2-}$, [a]	8.64×10^{-6}	1.09×10^{-3}	3.69×10^{-4}
$NiHCit^-$	2.84×10^{-4}	2.73×10^{-4}	1.58×10^{-4}
$Ni(NH_3)_3^{2+}$	1.19×10^{-5}	1.28×10^{-5}	2.50×10^{-5}
$Ni(NH_3)_4^{2+}$	1.23×10^{-5}	8.99×10^{-5}	1.76×10^{-5}
$Ni(NH_3)_2^{2+}$	3.86×10^{-6}	5.26×10^{-6}	1.03×10^{-5}
$Ni(NH_3)_5^{2+}$	4.64×10^{-6}	2.29×10^{-6}	4.48×10^{-6}
$Ni(NH_3)^{2+}$	4.09×10^{-7}	6.68×10^{-7}	1.31×10^{-6}
$Ni(NH_3)_6^{2+}$	3.82×10^{-6}	1.11×10^{-7}	2.17×10^{-7}
$NiOH^+$	1.88×10^{-5}	7.06×10^{-8}	1.38×10^{-7}
NiH_2Cit	1.97×10^{-8}	4.33×10^{-9}	7.37×10^{-8}
Ni^{2+}	1.30×10^{-8}	2.39×10^{-8}	4.68×10^{-8}
$Ni(OH)_2$	1.19×10^{-8}	8.48×10^{-11}	1.66×10^{-9}
$NiHPO_4$	5.33×10^{-12}	5.28×10^{-12}	5.02×10^{-10}
$Ni(OH)_3^-$	8.81×10^{-14}	1.61×10^{-13}	3.16×10^{-13}
PO_4^{3-}	1.84×10^{-6}	1.84×10^{-6}	4.81×10^{-5}
$\left[Ni^{2+}\right]^3\left[PO_4^{3-}\right]^2$	$10^{-35.1}$	$10^{-34.3}$	$10^{-30.6}$

[a] In [19] the calculations are for the dimer of this ion $\left(Ni_2Citr_2^{4-}\right)$

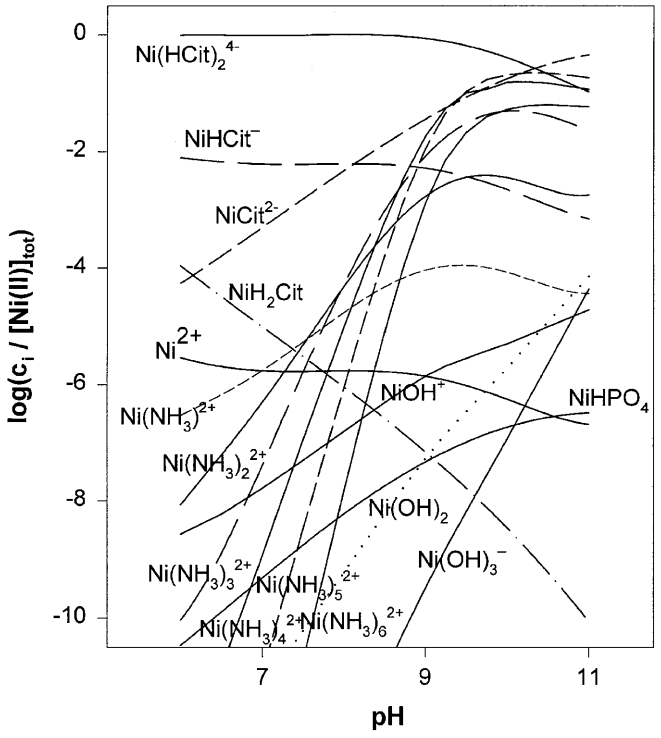

Fig. 2 Calculated molar fractions of Ni(II) complexes in total Ni(II) plotted versus pH. Solution composition: $[Ni(II)]_{tot} = 0.02$ mol/dm^3, $[H_3PO_4] = 0.014$, $C_{Cit,tot} = 0.2$ mol/dm^3. Calculations were done using published stability constants of Ni complexes [20] and corrected for the ionic strength of 2 mol/dm^3

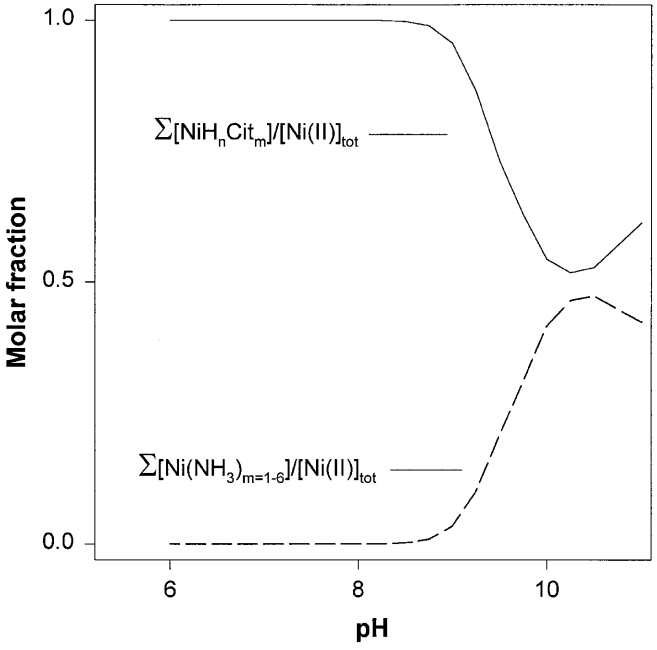

Fig. 3 Cumulated molar fractions of all citric and all ammonia nickel complexes in total Ni(II) plotted as functions of pH

two groups of these complexes plotted versus pH are shown in Fig. 3. The fraction of the ammonia complexes increases substantially for pH values higher than 9. For pH values higher than 10, an increase in the $NiCit^{2-}$ concentration takes place at the expense of the ammonia complexes. The calculated facts for the ammonia complexes were confirmed by spectrophotometric measurements (see Fig. 4). The spectra obtained at a pH lower than 9 are not affected by addition of phosphate ion or ammonia. At pH 10.7 (curve 5) the shape of the spectra is significantly changed. This change is caused by the formation of ammonia complexes, since the spectrum is identical to that obtained for a solution of $NiSO_4$ and ammonia (curve 7). Increase of the pH to more than 10 was expected to result in an increase in the molar fraction of the hydroxy complexes of Ni(II) in the solution. However, this fact was not confirmed by the spectrophotometric experiments.

The next step in the work was to determine how such factors as pH and the concentrations of other bath components influence the solubility, S, of $NiSO_4$ in the bath. For this purpose, partial derivatives $(\partial S/\partial C_i)_{Cj}$ and $(\partial S/\partial \mathrm{pH})_{Cj}$, where C_i is the concentration of species i in the bath, have been analyzed. The other concentrations were kept constant. It was found that the solubility of Ni(II) strongly depended on total concentration of citrates, $C_{Cit,tot}$. This is simply because most of the Ni(II) present in the bath solution is in the form of various citric complexes [~99% of total Ni(II) at pH in the range 8–8.5]. The dominating form is the complex $Ni(HCit)_2^{4-}$. At pH 8.5, $(\partial S/\partial C_{Cit,tot}) = 0.152$, which indicates that the solubility of $NiSO_4$ increases with an increase in the total citrate concentration. For example, the increase in the total concentration of the citric

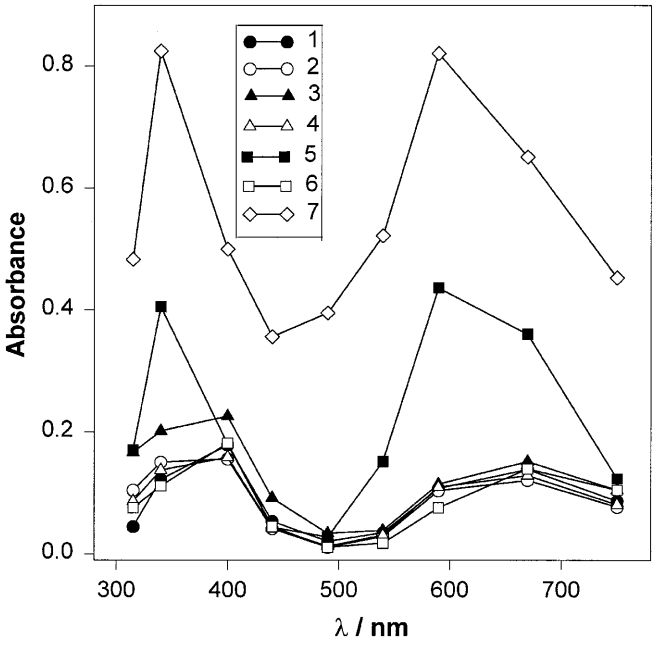

Fig. 4 Absorbance spectra in 0.02 mol/dm^3 Ni(II) solutions. Solution composition: 0.135 mol/dm^3 Na_2H_2Cit + 0.065 mol/dm^3 H_4Cit + 0.02 mol/dm^3 $NiSO_4$ (*1*); as (*1*), pH 8.42 (*2*); as (*1*), pH 10.72 (*3*); as (*1*) + NH_3, pH 8.42 (*4*); as (*1*) + NH_3, pH 10.7 (*5*); as (*1*) + 0.014 mol/dm^3 H_3PO_4 (*6*); $NiSO_4$ + NH_3, pH 10.06 (*7*). Curves *2* and *3*: pH was adjusted by addition of NaOH

species from 0.2 to 1.2 mol/dm^3, at pH 8.5, makes the solubility of $NiSO_4$ in the bath increase by approximately 10 times. The dependence of $NiSO_4$ solubility on total citrate concentration, $C_{Cit,tot}$ (at pH 8.5, and for 0.014 mol/dm^3 H_3PO_4 and 0.415 mol/dm^3 ammonia), can be expressed by the following equation:

$$S = 0.000046 + 0.094C_{Cit,tot} + 0.147C^2_{Cit,tot} \quad (1)$$

Equation 1 was obtained by employing the least-squares fitting procedure to the results of the calculations of S. This equation is parabolic, since the dominating complex at pH 8.5 is $Ni(HCit)_2^{4-}$ and the dependence of the $HCit^{3-}$ concentration on total citrate concentration (for solutions saturated with $NiSO_4$, at pH 8.5, and containing 0.014 mol/dm^3 H_3PO_4 and 0.415 mol/dm^3 ammonia) is also parabolic:

$$[HCit^{3-}] = 0.81C_{Cit,tot} - 0.29C^2_{Cit,tot} \quad (2)$$

The next factors that influence the solubility of $NiSO_4$ are pH and the concentration of the hydrogen phosphate species. With pH change in the range 7.5–9.5 the solubility of $NiSO_4$ changes by 10% only. Regarding the hydrogen phosphate species, the solubility of $NiSO_4$ increases with decreasing total H_3PO_4 concentration. For example, at pH 8.5 the decrease of the H_3PO_4 concentration from 0.11 mol/dm^3 to 0.014 mol/dm^3 increases the solubility of $NiSO_4$ by 20%. The other substances have a much smaller influence on the solubility of $NiSO_4$ in the bath.

It is known that the pH of the plating bath is one of the key parameters responsible for a good quality of the deposit. To keep the pH stable, the buffer capacity should be sufficiently large. We found that the presence of ammonia at a concentration of 0.415 mol/dm^3 increased the buffer capacity about 1.5–2 times at pH values above 9 and for concentrations of citrates in the range 0.2–1.2 mol/dm^3. The maximum buffer capacity was obtained at pH values in the range from 9.7 to 10, and a local minimum was found at pH 8.5, which unfortunately is the initial pH of the bath. Fortunately, since intensive hydrogen evolution takes pace during the electrodeposition, a possible increase in pH should be slow, as this increase is accompanied by a large increase in the buffer capacity.

As already mentioned, only two nickel compounds can precipitate from the plating bath solution: $Ni(OH)_2$ and $Ni_3(PO_4)_2$. The pH at which the precipitation of these compounds starts depends on the total citrate and the Ni(II) concentrations. This is shown in Fig. 5. The precipitation of $Ni(OH)_2$ always starts at a higher pH value than that of $Ni_3(PO_4)_2$. The solution remains stable below each line, indicating the precipitation of $Ni_3(PO_4)_2$.

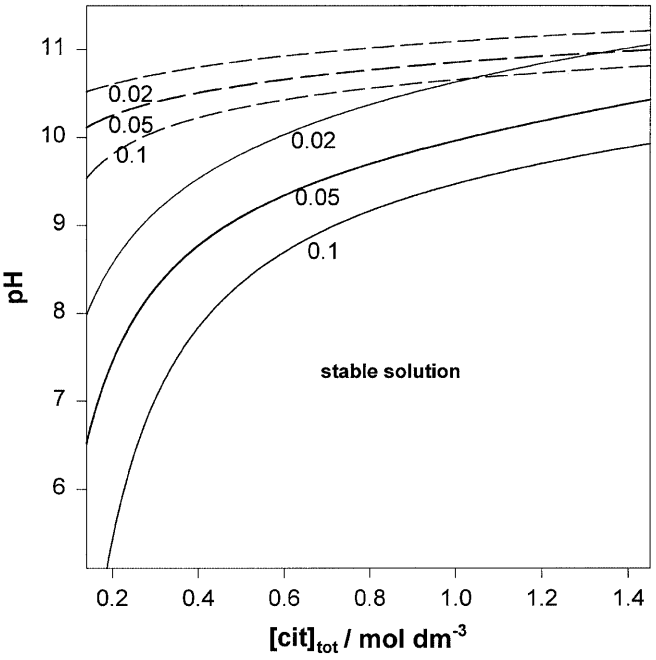

Fig. 5 Calculated pH for the start of precipitation of $Ni_3(PO_4)_2$ (*solid line*) and $Ni(OH)_2$ (*dotted line*) as a function of the total concentration of citrates in the solution containing H_3PO_4 (0.014 mol/dm^3), ammonia (0.415 mol/dm^3) and H_3BO_3 (0.365 mol/dm^3). The total concentration of Ni(II) is indicated below each curve

Electrodeposition rate of Ni-W alloys

To learn about the influence of Ni(II) concentration in the bath on the rate of Ni-W alloy electrodeposition, we have performed experiments with higher concentrations of citric compounds ($[Na_2H_2Cit] = 0.8$ mol/dm^3 and $[H_4Cit] = 0.4$ mol/dm^3). The increased concentration of the citrate species resulted in an increase in the solubility of $NiSO_4$ in the bath up to 0.163 mol/dm^3. In the consecutive electrodepositions the concentration of Ni(II) was changed in the range from 0.017 to 0.150 mol/dm^3. The amounts of the other components were kept at the level corresponding to the initial solution. The experimentally obtained deposition rates are plotted in Fig. 6. The deposition rate of the alloy increased significantly under the new conditions, especially for the higher current densities (curves 2 and 3). We want to stress here that under the conditions of constant current plating an increased deposition rate must be accompanied by an appropriate increase in the current efficiency, since the sum of the electrolysis charges of Ni, W and H is constant. This increase in current efficiency amounts to 32% against 8–12% for the initial solution; see Table 2.

The side effect of the increase in the concentration of the citric compounds from 0.2 mol/dm^3 to 1.2 mol/dm^3 is a decrease in the tungsten content. For the total concentration of Ni(II) equal to 0.02 mol/dm^3 and $i = 35$ and 100 mA/cm^2, the tungsten content decreases to 14.2 and 15.5 at%, respectively. This is illustrated in Fig. 7. All the dependencies presented in Fig. 7 have a maximum at a Ni(II) concentration of approximately 0.04–0.05 mol/dm^3, so this concentration of Ni(II), from the point of view of maximum W content and the maximum deposition rate, seems to be optimal. The amorphous-

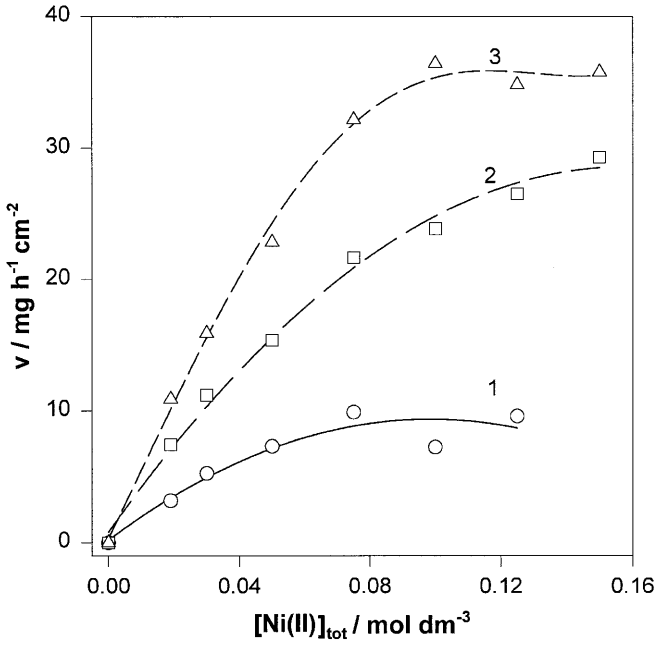

Fig. 6 Effect of total Ni(II) concentration on alloy deposition rate, v, for various current densities: $i = 35$ (*1*); 70 (*2*); 100 mA/cm^2 (*3*). Solution composition: $[Na_2H_2Cit] = 0.8$ mol/dm^3, $[H_4Cit] = 0.4$ mol/dm^3, pH 8.5. Concentrations of other components are the same as in the initial solution

ness of the alloys (the size of the nanocrystals) is also affected under the conditions of the increased electrodeposition rate of nickel. This is discussed in the next section.

X-ray spectra and size of the nanocrystals

The increase in the current efficiency and in the deposition rate, obtained by increasing the concentration of the nickel species in the solution, is accompanied by some changes in the X-ray diffraction patterns. As is seen in Fig. 8, curve 1, a broad maximum typical for the amorphous Ni-W structure is placed at the 2Θ angle of ca. 55.8°, which value is slightly less than that known for the Ni(111) signal. The alloy signal becomes more steep as the tungsten content in the alloy decreases to between 15 and 14 at% (curves 2 and 3 in Fig. 8). At this W content, only one diffraction signal is observed. The steeper shape of the diffractograms indicate that the order range in the deposited layers is increased, while the absence of more reflections originating from the other surfaces means that the layers contain just one phase with the (111) planes parallel to the substrate surface. The diffractograms obtained for the alloys containing 12 and 10 at% W exhibit further changes. Not only the intensity of the signal decreases and its half-width drops, but at the same time, two other weak signals located close to the Ni(200) and Ni(220) lines appear in the diffractograms. This is illustrated by curves 4 and 5 in Fig. 8. Apparently the internal structure of the alloys starts to resemble, a little, the structure of the polycrystalline nickel. A little, since the diffraction signals are of rather low intensity. We conclude that the alloy structure remains virtually homogeneous and amorphous-like.

To characterize the amorphous structure more quantitatively, one should rather speak about the size of the nanocrystals [11]. We have done this by correlating the broadening of the diffraction peaks and the grain size in the alloy layers. For the calculation, we have used the formula given originally by Scherrer [21]: $\beta = 0.94\lambda/(\epsilon \cos\Theta)$, where β is the peak broadening in radians, λ is the wavelength in Å, ϵ is the crystal size in Å and Θ is the position of the peak on the diffractogram. The digital constant 0.94 in the above expression for β is the best for the cubic structure. The corrected definition of the line broadening, $\beta^2 = B^2 - b^2$, where b is the width of the peak for the crystalline material and B is the peak width of the sample examined, was given by Warren and Biscoe [22]. In our case, the value of b was experimentally determined for the Ni(111) peak of the polycrystalline nickel. The number obtained was 0.00872 radians. The sizes of the nanocrystals present in the amorphous alloy layers, calculated from the peak broadening, are presented in Table 3.

Conclusions

The experimental data obtained indicate clearly that it is possible to control the key parameters of the amor-

Table 2 Current efficiencies obtained for various concentrations of $NiSO_4$ in the initial solution modified by increasing the total citrate concentration to 1.2 mol/dm^3

Concentration of $NiSO_4$ in the bath (mol/dm^3)	Current efficiency (%)		
	35 mA/cm^2	70 mA/cm^2	100 mA/cm^2
0.017	–	9.6	–
0.019	8.3	–	9.1
0.030	13.6	14.5	14.4
0.050	18.9	19.9	20.6
0.075	25.6	28.0	29.2
0.100	18.8	30.9	33.0
0.125	23.0	32.1	31.0
0.150	22.5	32.3	33.0
Initial solution: $C_{Cit,tot} = 0.2$ M, $[NiSO_4] = 0.02$ M	12.2	9.9	8.9

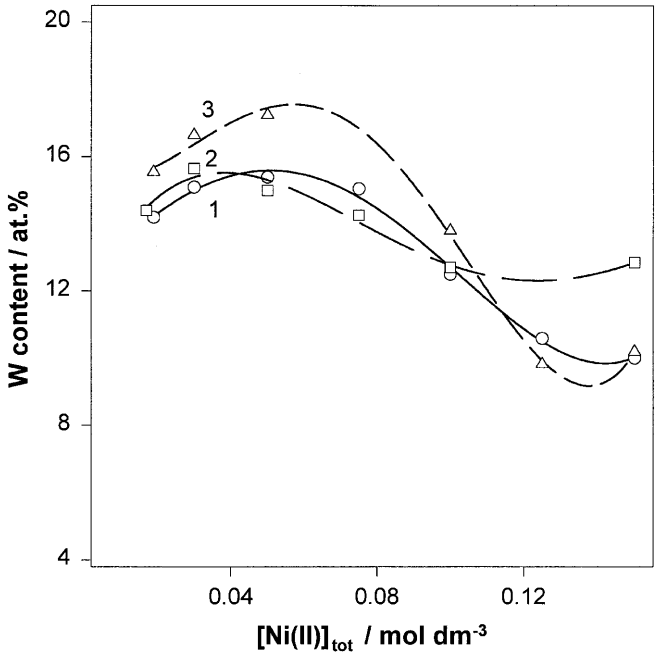

Fig. 7 Influence of $NiSO_4$ concentration on tungsten content for various current densities. Solution composition: as in Fig. 6

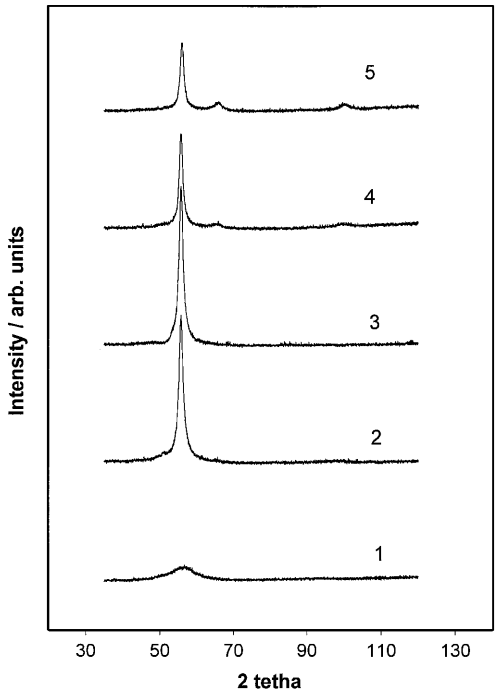

Fig. 8 X-ray diffractograms obtained for Ni-W alloys deposited in: the initial solution (*1*), and solutions containing increased concentrations of Ni: 0.03 (*2*); 0.05 (*3*); 0.075 (*4*); 0.125 mol/dm^3 (*5*). Total citrate concentration: 1.2 mol/dm^3 (*2–5*); current density: 70 mA/cm^2

phous/nanocrystalline Ni-W alloys using the appropriate concentrations of citrate and Ni(II) in the bath. The increase in the concentration of citrate followed by the corresponding increase in the nickel concentration, at the optimal pH of 8.5, results in a significant increase, by 3.2 times, in the deposition efficiency and therefore the deposition rate of the alloys. At the same time, a decrease in the tungsten content takes place and the order range in the alloy deposits increases. Interestingly, at this enhanced deposition rate, the Ni-W alloy is still rather more amorphous than polycrystalline, as the width of the peak in the diffractograms is substantially larger compared to the polycrystalline nickel. The sizes of the nanocrystals estimated from the peak width using the Scherrer formula equaled 15–100 Å, depending on the nickel concentration and the deposition rate. Only the number obtained for alloy 1 can be compared with the literature data: Yamasaki [13] examined a similar electrodeposited alloy and obtained a grain size in the range 25–68 Å by analyzing the X-ray diffractograms, and in the range 30–70 Å by transmission electron microscopy. His alloys were, however, obtained under conditions of much higher current density, and the tungsten content did not cover the range of concentrations of this report.

Since only one peak is seen in the X-ray diffractograms, we presume that the alloy is homogeneous. Also, since the peak maximum is located close (at 2Θ = ca. 55.8°) to the (111) peak of fcc Ni, we conclude that this structure of Ni, somewhat deformed, is dominating in the alloy layers, and the (111) planes are parallel to the substrate surface. Interestingly, the alloys marked as 2 and 3 in Table 3 maintain the deposit hardness of alloy 1 despite the decrease in the tungsten content. We believe the similarity of the structure of these alloys is responsible for the unchanged hardness. In fact, the hardness of alloys 2 and 3 is even slightly higher than that of alloy 1, which is maximally amorphous. Alloys 2 and 3 were obtained from the solutions containing an increased concentration of Ni(II) (by 2–3 times). A further in-

Table 3 Size of crystals and other parameters for the layers of Ni-W alloys electrodeposited under various conditions. Solution composition: alloy 1, initial solution; alloys 2–5, total concentration of citrate ions was increased to 1.2 mol/dm^3

Alloy no.	$C_{Ni(II)}$ (mol/dm^3)	Deposition rate (mg/h/cm^2)	Current efficiency (%)	Composition W:Ni (at%)	Half-peak width (radians)	Estimated grain size (Å)	Hardness (HV)
1	0.02	7.69	9.9	19.5:80.5	0.136	15	824
2	0.03	11.22	14.5	14.8:85.2	0.0241	84	840
3	0.05	15.39	19.9	13.9:86.1	0.0230	87	832
4	0.075	21.60	28.0	11.9:88.1	0.0204	100	728
5	0.125	24.65	32.1	10.0:90.0	0.0218	90	684

crease in the Ni(II) concentration in the plating bath leads to a decrease in the tungsten content down to 10 at%. This is accompanied by a decay in the preferred (111) surface orientation and a significant lowering of the hardness. While sample 5 obtained from the solution of the highest concentration of Ni(II) is still much harder than the pure nickel deposited from the citrate baths (ca. 350 HV) [23], its smoothness and the adhesion to the substrate is worse.

An important final conclusion is that that it is possible, by changing the citrate and nickel concentrations, to increase the alloy deposition rate and to obtain amorphous/nanocrystalline deposits of various grain size, various compositions and similar good appearance and high hardness.

Acknowledgements This work was partially supported by the Ministry of Education and Science of Lithuania, and by a Warsaw University grant no. BST 662/5/2000.

References

1. Donten M (1999) J Solid State Electrochem 3:87
2. Yao S, Zhao S, Guo H, Kawasaka M (1996) Corrosion 52:183
3. Donten M, Gromulski T, Stojek Z (1998) J Alloys Compd 279:272
4. Donten M, Stojek Z, Osteryoung JG (1993) J Electrochem Soc 140:341
5. Donten M, Osteryoung JG (1991) J Appl Electrochem 21:496
6. Donten M, Stojek Z (1994) Pol J Chem 68:1193
7. Ikeda H, Ioku S, Fuita T, Maenaka K, Maeda M (1999) Trans Inst Elect Eng Jpn E 119:598
8. Younes O, Gileadi E (2000) Electrochem Solid-State Lett 3:543
9. Obradovic M, Stavanovic J, Stevanovic R, Despic A (2000) J Electroanal Chem 491:188
10. Bratoyeva M, Atapason N (2000) Sov Electrochem 36:69
11. McHenry ME, Willard MA, Laughlin DE (1999) Prog Mater Sci 44:291
12. Croopnick GA, Scruggs DM (1985) US Pat 4 529 668
13. Yamasaki T (2000) Mater Phys Mech 1:127
14. Donten M, Cesiulis H, Stojek Z (2000) Electrochim Acta 45:3389
15. Kanapeckaite S, Survila A (1993) Chemija 2:22 (in Russian)
16. Lurje Ju (1979) Handbook of analytical chemistry. Khimija, Moscow (in Russian)
17. Ishikawa M, Enomoto H (1989) J Surf Finish Soc Jpn 40:1266
18. Green TA, Russell AE, Roy S (1998) J Electrochem Soc 145:875
19. Beltowska-Lehman E, Ozga P (1998) Electrochim Acta 43:617
20. Martell AE, Smith RM (1977) Critical stability constants. Plenum Press, New York
21. Scherrer P (1918) Nachr Ges Wiss Goettingen 98
22. Warren BE, Biscoe JB (1938) J Am Ceram Soc 21:49
23. Chein-Ho Huang (1997) Plating Surf Finishing 84:62